Supporting Information

The post-treatment effects on open circuit voltages and device performances in a high efficiency all-small-molecule organic solar cell

Ziqi Zhang,[ab#] Qiong Wu,[ab#] Dan Deng,[*a] Sihua Wu, [ab] Rui Sun,[c] Jie Min,[c] Jianqi Zhang,[a] and Zhixiang Wei[*ab]

Contents

1 Materials and synthesis

2 Characterization

3 Cyclic voltammograms of BSCl and IDIC-4Cl

4 GIWAXS tests for BSCl, BSCl-C2 and IDIC-4Cl film

5 Device optimization for ASM-OSCs

6 Bandgap energy measurement for BSCl:IDIC-4Cl blend films

7 FTPS-EQE tests for ASMOSCs

8 UPS tests for pristine BSCl film and BSCl:IDIC-4Cl blend films

9 References

1 Materials and synthesis

All chemicals and solvents were purchased from J&K, Alfa Aesar, Aldrich, Aladdin, Macklin and Beijing Chemical Plant. Toluene was freshly distilled prior to use. Compound 1 was obtained Hyper chemical company. **IDIC-4Cl** (2,2'-((2Z,2'Z)-((4,4,9,9-tetraoctyl-4,9-dihydro-s-indaceno[1,2-b:5,6-b']di-thiophene-2,7diyl)bis(methanylylidene))bis(5,6-dichloro-3-oxo-2,3-dihydro-1H-ind-ene-2,1-diylidene))dimalononitrile), **compound 2** (5-(5-bromo-6-hexylthieno[3,2-b]thiophen-2-yl)-4-

hexylthiophene-2-carbaldehyde) and rhodanine with different alkyl chains were prepared according our previous work and the literature.[1-3] And the detailed synthetic processes of donors were illustrated as follows.

Scheme S1. The synthetic routes of BSCl
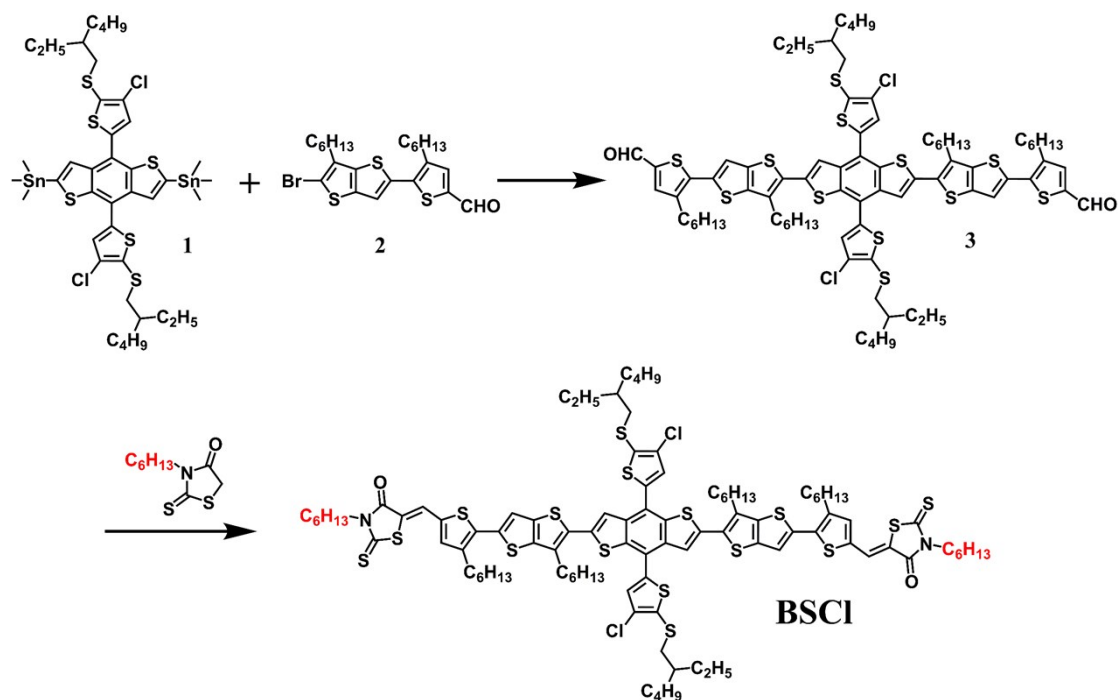
Compound 3 (5,5'-(5,5'-(4,8-bis(4-chloro-5-((2-ethylhexyl)thio)thiophen -2-yl)benzo[1,2-b:4,5-b']dithiophene-2,6-diyl)bis(6-hexylthieno[3,2-b]thiophene-5,2-diyl))bis(4-hexylthiophe-ne-2-carbaldehyde))

Compound 1 (0.7 g, 0.67 mmol), compound 2 (1 g, 2.02 mmol) and 50 mL dried toluene were mixed into a three necked flask. Under an Ar atmosphere at 0 ℃, Pd(PPh$_3$)$_4$ was added into the mixed solution. Then purging for another 15 min with Ar, the solution was heated to 110 ℃ and stirred for 18 h. After cooling to room temperature, the solvent was removed by rotary evaporation, and the crude product was purified by silica gel column chromatography with petroleum and dichloromethane (1:2) and precipitation in methanol. The product was obtained as red solid (620 mg, yield 60%). ^{1}H NMR (400 MHz, CDCl$_3$, ppm): δ 9.86 (s, 2H), 7.64 (s, 2H), 7.62 (s, 2H), 7.40 (s, 2H), 7.37 (d, 2H), 2.99 (t, 8H), 2.86 (t, 4H), 1.80 (m, 4H), 1.71 (m, 4H), 1.65 (m, 2H), 1.63–1.43 (m, 16H), 1.33–1.31 (m, 24H),0.96–0.87 (m, 24H), MALDI-TOF MS (*m/z*): 1545.3.

BSCl ((5E,5'E)-5,5'-((5,5'-(5,5'-(4,8-bis(4-chloro-5-((2-ethylhexyl)thio)thiophen-2-yl)benzo[1,2-

b:4,5-b']dithiophene-2,6-diyl)bis(6-hexylthieno[3,2-b]thiophene-5,2-diy l))bis(4-hexylthiophene-5,2-diyl))bis(methanylylidene))bis(3-hexyl-2-thioxothiazolidin -4-one))

Under the protection of Ar, 1 mL piperidine was dropped into the mixture of compound 3 (200 mg, 0.13 mmol), rhodanine[4] (281 mg, 1.3 mmol) and 30 mL dried chloroform. Then the system was heated to 70 °C and refluxed for 12 h. After the reaction, the mixture was settled out by methanol. The crude product was purified with column chromatography on silica gel with dichloromethane and petroleum (1:1). Then it was recrystallized with chloroform and methanol to yield the target material (136 mg, 54%) as a dark solid. ^{1}H NMR (400 MHz, CDCl$_3$, ppm): δ 7.76 (s, 2H), 7.62 (s, 2H), 7.37 (s, 2H), 7.36 (s, 2H), 7.23 (s, 2H), 4.09 (t, 4H), 3.00 (d, 8H), 2.84 (t, 4H), 1.82-1.78 (m, 2H), 1.70–1.66 (m, 12H), 1.54–1.33 (m, 52H), 0.90 (m, 30H). ^{13}C NMR (101 MHz, CDCl$_3$) δ 192.15, 167.50, 142.49, 141.64, 139.77, 139.45, 139.07, 138.33, 138.00, 136.96, 136.68, 135.88, 133.33, 132.76, 131.53, 129.86, 128.84, 124.62, 122.17, 120.95, 118.95, 99.99, 44.88, 42.10, 39.37, 32.21, 31.61, 31.58, 31.35, 30.25, 29.49, 29.21, 29.03, 28.81, 26.95, 26.46, 25.42, 22.96, 22.64, 22.61, 22.51, 14.12, 14.08, 14.02, 10.87, -0.00. MALDI-TOF MS (*m/z*): 1943.9. Anal. Calcd. (%) for C$_{98}$H$_{122}$N$_2$O$_2$S$_{16}$Cl$_2$: C, 60.43; H, 6.31; N, 1.48; S, 26.03. Found: C, 60.44; H, 6.30; N, 1.48; S, 26.04.

2 Characterization

Molecular properties characterization

The UV-Vis spectra for solution and films were obtained by Perkin Elmer Lambda950 spectrophotometer. The cyclic voltammetry (CV) measurement was carried out by an electrochemical workstation (VMP3 Biologic, France) with Pt electrode coated with target films, Pt plate and Ag/Ag$^+$ electrode acting as the working, counter, and reference electrodes, respectively, in a 0.1 mol L^{-1} tetrabutylammonium phosphorus hexafluoride (Bu$_4$NPF$_6$) acetonitrile solution. Redox potentials were calibrated using the ferrocene/ferrocenium (Fc/Fc$^+$) redox couple (−4.8 eV). Ultraviolet photoelectron spectroscopy (UPS) was carried out by AXIS ULTRA DLD multi-functional photoelectron spectrometer.

Fabrication and characterization of ASMOSCs

The devices were fabricated with a conventional structure of ITO/PEDOT:PSS/active layer/Al. The ITO-coated glass substrates were washed with detergent, deionized water, acetone and isopropanol in an ultrasonic bath for 30 minutes sequentially. Then the washed ITO glass was treated by UV-ozone

for 15 minutes. PEDOT:PSS was spin-coated onto ITO at 3500 rpm for 30 seconds and then annealed at 150℃ for 15 minutes. Donor and acceptor materials were dissolved in chloroform (CF) solvent with a total concentration of 15 mg/ml and then stirred at 50℃ for 30 minutes. The blend solution was spin-coated at 1050 rpm for 30 seconds to form a thin film on the substrate. Then alcohol was coated on the top of active layer at 3000 rpm for 35 seconds. Post-treatment such as thermal annealing and solvent vapor annealing were utilized to optimize the morphology of the active layer. Finally, a 80 nm of Al was deposited onto the active layer to form a back electrode.

One solar cell device consists of four cells and the active area of each cell was ca. 4 mm^2. The whole photovoltaic performance characterization was processed in a N$_2$-filled glovebox. Newport Thermal Oriel 91159 A solar simulator was used for J–V curves measurement under AM 1.5 G, and the light intensity was calibrated with Newport Oriel PN 91150 V Si-based solar cell. J–V measurement signals were recorded by Keithley 2400 source-measure unit. Oriel Newport system (Model 66902) was used for external quantum efficiency (EQE) measurements.

Charge carrier mobility characterization

Hole and electron mobilities were measured by the space-charge limited current (SCLC) method with hole-only devices and electron-only devices. The hole-only devices adopted ITO/PEDOT:PSS/active layer/MoO$_x$/Ag structure, while electron-only devices adopting ITO/ZnO/active layer/Ca/Al structure. The active layers for these two devices were spin-coated under the same condition as that of solar cells. J–V curves in the range of 0 to 5 V were gained by Keithley 2400 source-measure unit in the dark condition.

The mobilities were obtained by fitting J-V curves with the formula of:

$$J = \frac{9\varepsilon_0\varepsilon_r\mu V^2}{8L^3}exp(0.89\beta\sqrt{\frac{V}{L}})$$

where J is the current density, L is the thickness of the active layer, μ is the mobility, ε_0 is the vacuum dielectric constant, ε_r is the relative dielectric constant of the transport medium, V (= V_{app} - V_{bi}) is the internal voltage, where V_{app} is the applied voltage and V_{bi} is the built-in voltage.

Morphology and crystallization characterization

Transmission electron microscopy (TEM) characterization was performed by Tecnai G2 F20 U-TWIN TEM instrument. Grazing incidence wide angle x-ray scattering (GIWAXS) measurement was conducted at XEUSS SAXS/WAXS equipment.

Energy loss characterization

Electroluminescence (EL) sepctra were obtained by applying an external current source through the devices powered by Keithley 2400 source meter, the emitted light was recorded with a Si CCD detector installed inside the Zolix Flex One Spectrometer.

The Fourier-transform photocurrent spectroscopy external quantum efficiency (FTPS-EQE) measurements were performed with a modified Bruker Vertex 70 FTIR spectrometer equipped with a tungsten lamp and a quartz beam-splitter, using the solar cell as the external detector. A low noise current amplifier (Femto DLPCA-200) was used to amplify the photocurrent produced from solar cell. The output voltage of the current amplifier is fed back to the external detector port of the FTIR spectrometer.

According to Marcus theory, the EQE of solar cells (EQE_{PV}) at photon energy E is described by the following formula: [5]

$$EQE_{PV}(E) \cdot E = \frac{f}{\sqrt{4\pi\lambda kT}} exp(\frac{-(E_{CT} + \lambda - E)^2}{4\lambda kT})$$

Here, k is Boltzmann constant, T is the temperature in Kelvins, f is the oscillator absorption strength, E_{CT} is the charge transfer state energy, and λ is the reorganization energy.

The lower energy part of the FTPS-EQE spectra can be fitted by Marcus theory. Through the fitting curve, E_{CT}, λ, and f were finally obtained as parameters.

V_{oc}^{rad} is defined as the open-circuit voltage when there is only radiative recombination in the solar cell, which satisfies the following expression: [6]

$$V_{OC}^{rad} = \frac{kT}{q} \ln(\frac{J_{SC,rad}}{J_{0,rad}} + 1) = \frac{kT}{q} \ln(\frac{q\int_{E_g}^{\infty} EQE_{PV} \emptyset_{AM1.5}(E)\, dE}{q\int_{E_g}^{\infty} EQE_{PV} \emptyset_{BB}(E)\, dE} + 1)$$

Here, k is Boltzmann constant, T is the temperature in Kelvins, q is the elementary charge, EQE_{PV} is the external quantum efficiency of solar cells, $\emptyset_{AM1.5}$ is the solar radiation photon flux at 1 sun AM 1.5, and $\emptyset_{BB}$ is the black body radiation at 300 K.

Driving force represents the energy loss due to charge generation, which has the definition of $E_g -$ E_{CT}.[7] The driving force values the energetic offsets between the donor and acceptor, and it directly

effects the degree of singlet exciton transferring to CT state.
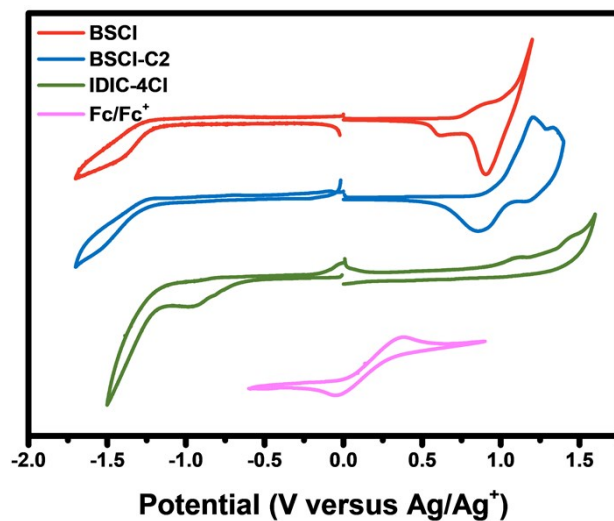
3 Cyclic voltammograms of BSCl, BSCl-C2 and IDIC-4Cl

Fig. S1 Cyclic voltammograms of BSCl, BSCl-C2 and IDIC-4Cl.

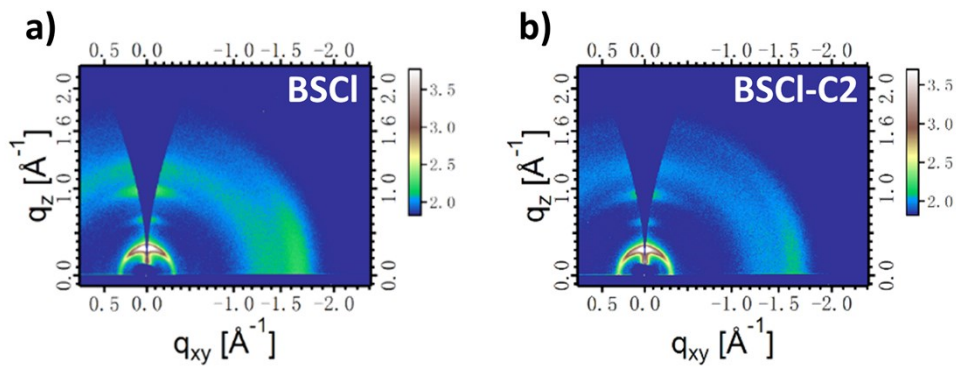## 4 GIWAXS tests for BSCl, BSCl-C2 and IDIC-4Cl film

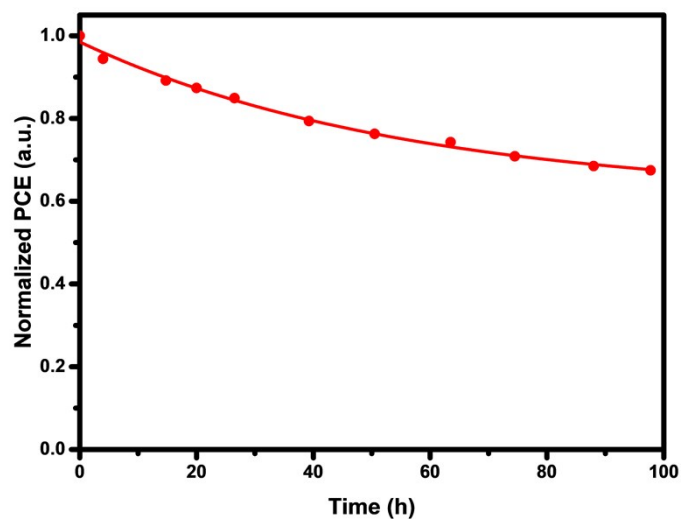**Fig. S2** 2D GIWAXS graphs of (a) BSCl and (b) BSCl-C2 film.

Fig. S3 Stability test of the SVA+TA device under nitrogen atmosphere at room temperature
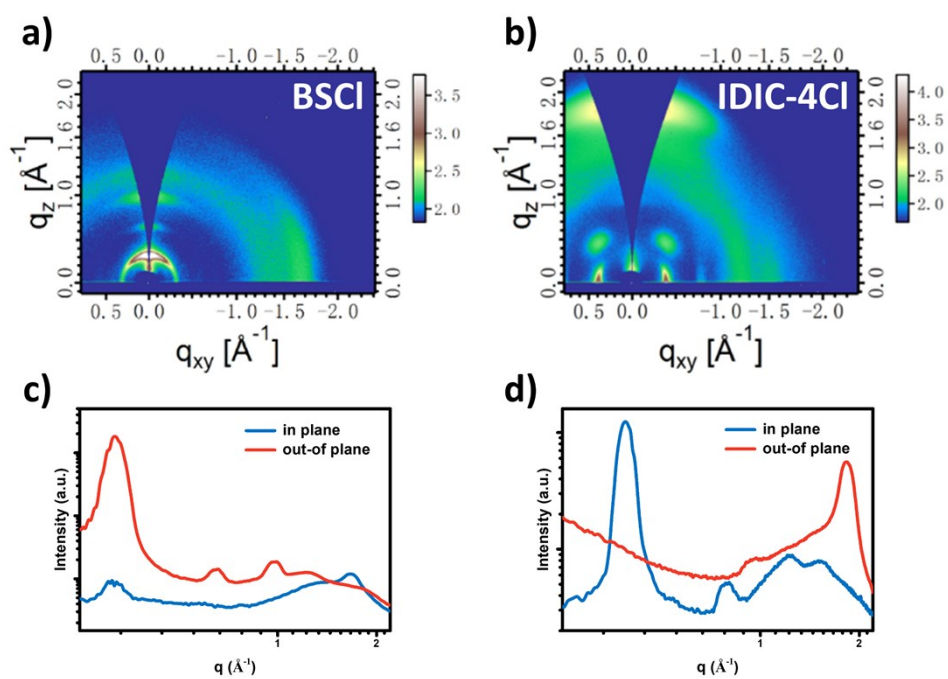

Fig. S4 2D GIWAXS graphs of pristine (a) BSCl and (b) IDIC-4Cl film; (c-d) corresponding in-plane and out-of-plane curves.

5 Device optimization for ASMOSCs

Table S1. Device optimization of annealing temperature for BSCl: IDIC-4Cl

TA temperature	V_{oc} (V)	J_{sc} (mA cm^{-2})	FF (%)	PCE (%)
as-cast	0.900	7.7	33.9	2.35
	(0.903±0.0058)	(7.5±0.35)	(34.4±1.50)	(2.32±0.024)
110 ℃	0.864	18.9	60.1	9.79
	(0.861±0.0028)	(17.3±0.93)	(62.9±2.63)	(9.35±0.244)
120 ℃	0.845	19.1	65.6	10.57
	(0.843±0.0025)	(18.4±0.71)	(66.3±2.52)	(10.25±0.236)
130 ℃	0.816	19.8	62.3	10.08
	(0.818±0.0043)	(19.6±0.56)	(61.5±1.91)	(9.85±0.188)

Fixed condition: D:A= 1:0.7(w/w), TA time= 10 min, rotation speed of spin-coating= 1050rpm, rotation time of spin-coating= 30s

Table S2. Device optimization of solvent vapor annealing time with THF for BSCl: IDIC-4Cl

THF SVA	V_{oc} (V)	J_{sc} (mA cm^{-2})	FF (%)	PCE (%)
as-cast	0.900	7.7	33.9	2.35
	(0.903±0.0058)	(7.5±0.35)	(34.4±1.50)	(2.32±0.024)
40 s	0.929	12.7	45.6	5.45
	(0.926±0.0026)	(12.0±0.80)	(45.3±0.54)	(5.02±0.406)
60 s	0.930	11.9	42.3	4.70
	(0.922±0.0074)	(11.0±0.65)	(42.9±1.60)	(4.35±0.209)
90 s	0.922	12.0	48.7	5.40
	(0.927±0.0033)	(11.1±0.82)	(44.8±2.30)	(4.64±0.506)

Fixed condition: D:A= 1:0.7(w/w), rotation speed of spin-coating= 1050rpm, rotation time of spin-coating= 30s

Table S3. Device optimization of D:A ratios for BSCl: IDIC-4Cl

D:A	V_{oc} (V)	J_{sc} (mA cm^{-2})	FF (%)	PCE (%)
1:0.6	0.877	19.8	72.0	12.15
	(0.876±0.0031)	(19.0±0.42)	(70.4±1.01)	(11.74±0.269)
1:0.7	0.865	21.5	70.0	13.03
	(0.864±0.0043)	(21.3±0.37)	(69.9±0.86)	(12.85±0.178)
1:0.8	0.870	20.0	68.9	11.97
	(0.868±0.0029)	(19.6±0.60)	(67.7±1.61)	(11.49±0.371)

Fixed condition: TA temperature= 120℃, TA time= 10 min, THF SVA time= 40s,

rotation speed of spin-coating= 1050rpm, rotation time of spin-coating= 30s

6 Bandgap energy measurements for BSCl: IDIC-4Cl blend films
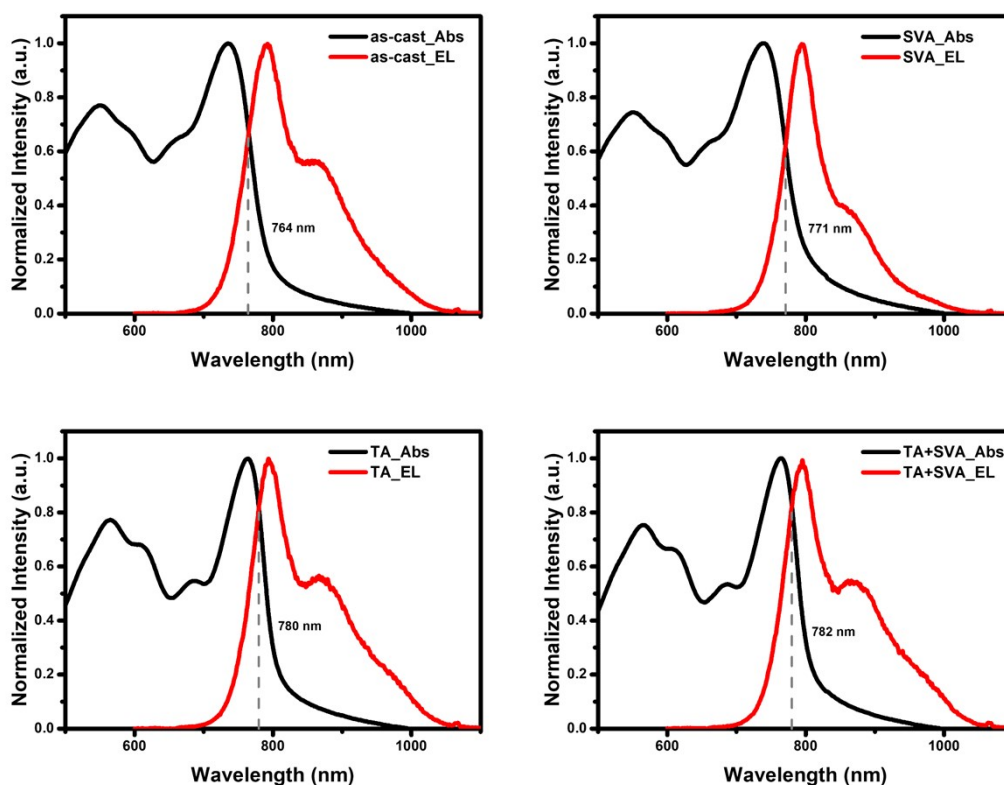
Fig. S5 Optical bandgap determined by the crossing point between the normalized absorption (black)

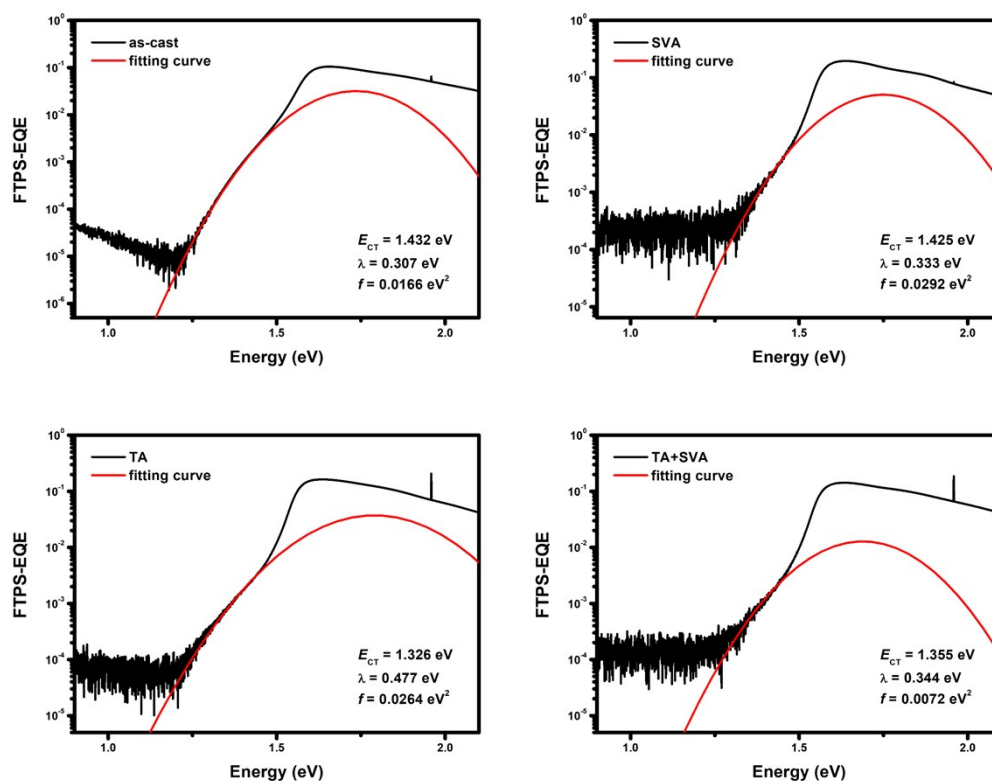and EL (red) spectra.

7 FTPS-EQE tests for ASMOSCs

Fig. S6 FTPS-EQE spectra (black) and corresponding fitting curve of Marcus theory (red) for BSCl:IDIC-4Cl blend films with different post-treatment.

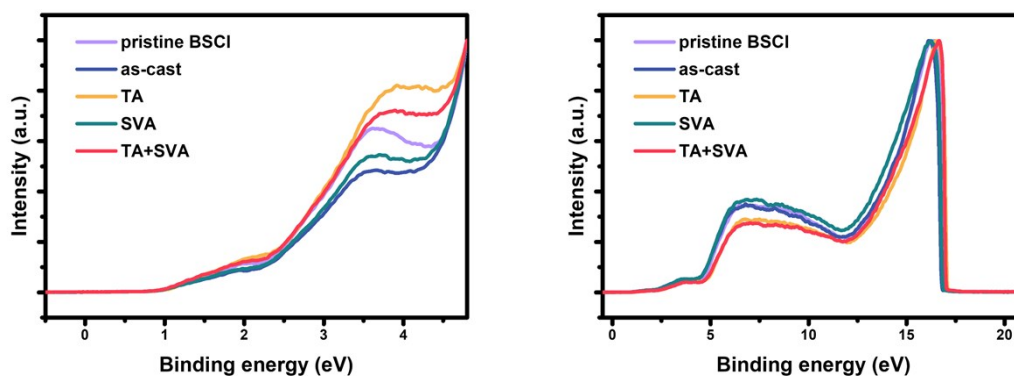## 8 UPS tests for pristine BSCl films and BSCl:IDIC-4Cl blend films

Fig. S7 UPS spectra of pristine BSCl film and BSCl:IDIC-4Cl blend films with different post-treatment.

9 Reference

1.   R. Zhou, Z. Jiang, C. Yang, J. Yu, J. Feng, M. A. Adil, D. Deng, W. Zou, J. Zhang, K. Lu, W. Ma, F. Gao and Z. Wei, *Nat. Commun.* 2019, **10,** 5393.

2.   D. Deng, Y. Zhang, J. Zhang, Z. Wang, L. Zhu, J. Fang, B. Xia, Z. Wang, K. Lu, W. Ma and Z. Wei, *Nat. Commun.* 2016, **7,** 13740.

3.   Q. Wu, D. Deng, R. Zhou, J. Zhang, W. Zou, L. Liu, S. Wu, K. Lu and Z. Wei, *ACS Appl. Mater. Interfaces*, 2020, **12**, 25100.

4.   L. Yang, S. Zhang, C. He, J. Zhang, Y. Yang, J. Zhu, Y. Cui, W. Zhao, H. Zhang, Y. Zhang, Z. Wei and J. Hou, *Chem. Mater.* 2018, **30**, 2129.

5.   K. Vandewal, K. Tvingstedt, A. G. Dinku, O. Inganas and J. Manca, *Phys. Rev. B*, 2010, **81,** 125204.

6.   D. Qian, Z. Zheng, H. Yao, W. Tress, T. R. Hopper, S. Chen, S. Li, J. Liu, S. Chen, J. Zhang, X.-K. Liu, B. Gao, L. Ouyang, Y. Jin, G. Pozina, I. A. Buyanova, W. M. Chen, O. Inganäs, V. Coropceanu, J.-L. Bredas, H. Yan, J. Hou, F. Zhang, A. A. Bakulin and F. Gao, *Nat. Mater.* 2018, **17**, 703.

7.   S. M. Menke, N. A. Ran, G. C. Bazan and R. H. Friend, *Joule*, 2018, **2**, 25.